Anticorrosively Enhanced PMMA−Clay Nanocomposite Materials with Quaternary Alkylphosphonium Salt as an Intercalating Agent

Jui-Ming Yeh,* Shir-Joe Liou, Ching-Yi Lin, Chiao-Yu Cheng, and Ya-Wen Chang

Department of Chemistry and Nano-material Research Center, Chung-Yuan Christian University, Chung Li, Taiwan 320, Republic of China

Kueir-Rarn Lee

Department of Chemical Engineering, Nanya Institute of Technology, Chung Li, Taiwan 320, Republic of China

Received April 18, 2001. Revised Manuscript Received July 5, 2001

A series of polymer−clay nanocomposite (PCN) materials that consisted of poly(methyl methacrylate) (PMMA) and layered montmorillonite (MMT) clay were prepared by effectively dispersing the inorganic nanolayers of MMT clay in an organic PMMA matrix via in situ thermal polymerization. Organic methyl methacrylate monomers were first intercalated into the interlayer regions of organophilic clay hosts followed by a typical free radical polymerization. The as-synthesized PCN materials were characterized by infrared spectroscopy, wide-angle powder X-ray diffraction, and transmission electron microscopy. PCN coatings with low clay loading (e.g., 1 wt %) on cold-rolled steel were found much superior in anticorrosion over those of bulk PMMA based on a series of electrochemical measurements of corrosion potential, polarization resistance, corrosion current, and impedance spectroscopy in 5 wt % aqueous NaCl electrolyte. The molecular weights of PMMA extracted from PCN materials and bulk PMMA were determined by gel permeation chromatography with tetrahydrofuran as an eluant. Effects of the material composition on the molecular barrier, optical clarity, and thermal stability of PMMA along with PCN materials, in the form of both free-standing film and fine powder, were also studied by molecular permeability analysis, ultraviolet−visible transmission spectra, differential scanning calorimetry, and thermogravimetric analysis, respectively.

Introduction

Polymeric (or organic) coatings have been employed to protect metals against corrosion for a long time. The primary effect of a polymeric coating is to function as a physical barrier against aggressive species such as O_2 and H^+. However, all polymeric coatings are not permanently impenetrable, and once there are defects in the coatings, pathways will be formed for the corrosive species to attack the metallic substrate and localized corrosion will occur. Therefore, as a second line of defense for corrosion, various pigments with a lamellar or platelike shape such as micaceous iron oxide and aluminum flakes have been introduced into the polymeric coating to effectively increase the length of the diffusion pathways for oxygen and water as well as decrease the permeability of the coating.[1]

A number of electrochemical measurements have been used as a tool to evaluate the anticorrosion performance of polymeric coatings including conjugated (e.g., polyaniline) or nonconjugated (e.g., polystyrene) polymers. For example, Wei et al.[2] demonstrated the anticorrosive performance of conjugated polyaniline and nonconjugated polystyrene by performing a series of electrochemical measurements of corrosion potential and corrosion current on the sample-coated cold-rolled steel (CRS) under various conditions. Lee and coworkers[1] investigated the corrosion-resistance properties of polyaniline-coated mild steel in saline and acid by electrochemical impedance spectroscopy.

Recently, montmorillonite (a layered material with lamellar shape) has attracted intense research interest for the preparation of polymer−clay nanocomposites because its lamellar elements display high in-plane strength, stiffness, and high aspect ratio. Typically, the chemical structures of montmorillonite (MMT) consist of two fused silica tetrahedral sheets sandwiching an edge-shared octahedral sheet of either magnesium or aluminum hydroxide. The Na^+ and Ca^{2+} residing in the interlayer regions can be replaced by organic cations such as alkylammonium ions by a cationic-exchange reaction to render the hydrophilic-layered silicate organophilic. The historical development of polymer−clay nanocomposites can be traced back to the work of

* To whom correspondence should be addressed.

(1) Li, P.; Tan, T. C.; Lee, J. Y. *Synth. Met.* **1997**, *88*, 237.

(2) Wei, Y.; Wang, J.; Jia, X.; Yeh, J.-M.; Spellane, P. *Polymer* **1995**, *36*, 4535.

10.1021/cm010337f CCC: $22.00
Published on Web 11/30/2001

polyamide−clay nanocomposites reported by Toyota's research group in 1990.[3] According to many recently published works, the dispersion of nanolayers of mineral clay was found to boost the thermal stability,[4] mechanical strength,[5] molecular barrier,[6] and flame-retardant[7] properties of polymers.

Recently, we reported that the dispersion of nanolayers of mineral clay was found to enhance the corrosion inhibition of polyaniline (a conjugated polymer) on a metallic surface via the formation of polyaniline−clay nanocomposite coatings on the basis of a series of electrochemical corrosion measurements of corrosion potential, polarization resistance, and corrosion current.[8]

In this paper, we present the first evaluation of the anticorrosive effect for the nonconjugated polymer−clay nanocomposite coatings, poly(methyl methacrylate) (PMMA)−clay, with a quaternary alkylphosphonium salt instead of a commonly used quaternary alkylammonium salt as the intercalating agent. The as-synthesized PCN materials were characterized by wide-angle powder X-ray diffraction, transmission electron microscopy, and infrared spectroscopy. PCN materials in the form of coatings with low clay loading on cold-rolled steel were found to be superior in anticorrosion over those of bulk PMMA on the basis of a series of electrochemical measurements of corrosion potential, polarization resistance, corrosion current, and impedance spectroscopy in 5 wt % aqueous NaCl electrolyte. Furthermore, we found that a further increase of clay loading results in a slightly further enhanced molecular barrier property of PCN materials. The effect of material composition on the molecular barrier, optical clarity, and thermal stability were also studied by molecular permeability analysis, ultraviolet−visible transmission spectra, differential scanning calorimetry (DSC), and thermogravimetric analysis (TGA), respectively.

Experimental Section

Chemicals and Instrumentations. Poly(methyl methacrylate) (M_w = 350 000) (Acros.), methyl methacrylate (Riedel-De Haen, 99%), benzoyl peroxide (Riedel-De Haen, 98%), 1-methylpyrrolidinone (Tedia, 99.6%), tetrahydrofuran for GPC (Fisher Scientific, 99.8%), tetrahydrofuran for reagent (Riedel-De Haen), lithium chloride (Acros., 99%), hydrochloric acid (Riedel-De Haen, 37%), *n*-hexane (Tedia, 85%), and toluene (Mallinckrodt, 99.8%) were used as received without further purification. Both quaternary alkylphosphonium salt, $Br^-P^+(Ph)_3CH_2CH_2N(CH_3)_2$ (Aldrich, 97%), and alkylammonium salt, 1-hexadecylamine (Acros, 90%), were used as intercalating agents. The montmorillonite clay, supplieded by Industrial Technology Research Institute (ITRI), was employed and had a unit cell formula of $Na^+_{0.31}[Al_{1.67}Mg_{0.33}]Si_4O_{10}(OH)_2 \cdot 5.8H_2O$ and a CEC value of 122 mequiv/100 g.

Wide-angle X-ray diffraction study of the samples was performed on a Rigaku D/MAX-3C OD-2988N X-ray diffractometer with a cooper target and Ni filter at a scanning rate of 4°/min. The samples for transmission electron microscopy (TEM) study was first prepared by putting the powder of PCN materials into PMMA resin capsules followed by curing of the PMMA resin at 100 °C for 24 h in a vacuum oven. Then, the cured PMMA resin containing PCN materials was microtomed with Reichert-Jumg Ultracut-E into 60−90-nm-thick slices. Subsequently, one layer of carbon about 10-nm thick was deposited onto these slices on mesh 100 copper nets for TEM observations on a JEOL-200FX with an acceleration voltage of 120 kV. FTIR spectra were recorded on pressed KBr pellets using a BIO-RAD FTS-7 FTIR spectrometer. A Perkin-Elmer thermal analysis system equipped with model 7 DSC and model 7/DX TGA was employed for the thermal analyses under air flow. The programmed heating rate was 20 °C/min in most cases.

Electrochemical measurements of corrosion potential, polarization resistance, corrosion current, and impedance spectroscopy on sample-coated CRS coupons were performed on a VoltaLab 21 and VoltaLab 40 potentiostat/galvanostat in a standard corrosion cell equipped with two graphite rod counter electrodes and a saturated calomel electrode (SCE) as well as the working electrode. The molecular weight of polymer extracted from all composite samples as well as bulk PMMA was determined on a Perkin-Elmer model TC4 equipped with a model 590 programmable solvent delivery module, a differential refractometer detector, and a Styragel HT column with THF as the eluant and monodispersed polystyrenes as calibration standards. A Yanagimoto Co., Ltd. gas permeability analyzer (model GTR 10) was employed to perform the permeation experiment of oxygen gas and water vapor. UV/vis transmission spectra were obtained using a Hitachi U-2000 UV/vis spectrometer.

Synthesis of Poly(methyl methacrylate). A typical procedure to prepare the poly(methyl methacrylate) is given as follows: 22.44 g (204 mmol) of methyl methacrylate (MMA), 2.48 g (10.2 mmol) of benzoyl peroxide (BPO), and 64 mL of dry toluene were put in a 250-mL three-neck round-bottom flask connected to a condenser, thermometer, and nitrogen gas inlet/outlet. Nitrogen gas was bubbled into the flask throughout the reaction. Under magnetic stirring, the solution was heated to 70 °C and maintained for 3 h. The reaction mixture solution was then poured into about 800 mL of hexane to precipitate the polymer. After filtration, the polymer was dissolved in 50 mL of dry toluene followed by reprecipitation in 800 mL of hexane. The purification procedure was repeated twice and the purified polymer was dried under vacuum at room temperature for 48 h. PMMA (20.0 g) was obtained in ≈60% yield.

Preparation of Organophilic Clay. The organophilic clay was prepared by a cation-exchange reaction between the sodium cations of MMT clay and quaternary alkylammonium cations ($CH_3(CH_2)_{15}NH_3^+$) or alkylphosphonium cations ($P^+(Ph)_3$-$CH_2CH_2CH_2N(CH_3)_2$) of intercalating agent. The equation for calculating the intercalating agent used for a cation-exchange reaction was listed as follows:

$$122/100 \times 5 \text{ g (for clay)} \times 1.2 = (X/M_w \text{ of intercalating agent}) \times 1 \times 1000$$

where X represents the amount of used intercalating agent, 122/100 represents the CEC value per 100 g of MMT clay, and 1.2 (>1) indicates the excess amount of intercalating agent used. Typically, 5 g of MMT clay with a CEC value of 122 mequiv/100 g was stirred in 400 mL of distilled water (beaker A) at room temperature overnight. A separate solution containing an excess amount of intercalating agent (2.45 g) in another 30 mL of distilled water (beaker B) was magnetically stirred, followed by the addition of 1 M HCl aqueous solution to adjust the pH value to about 3−4. After the solution was stirred for 1 h, the protonated amino acid solution (beaker B) was added at a rate of ≈10 mL/min with vigorous stirring to the MMT suspension (beaker A). The mixture was stirred overnight at room temperature. The organophilic clay was recovered by ultracentrifugating (9000 rpm, 30 min) and

(3) Usuki, A.; Kawasumi, M.; Kojima, Y.; Okada, A.; Karauchi, T.; Kamigaito, O. *J. Mater. Res.* **1993**, *8*, 1774.
(4) Lan, T.; Kaviratna, P. D.; Pinnavaia, T. J. *Chem. Mater.* **1994**, *6*, 573.
(5) Tyan, H.-L.; Liu, Y.-C.; Wei, K.-H. *Chem. Mater.* **1999**, *11*, 1942.
(6) Wang, Z.; Pinnavaia, T. J. *Chem. Mater.* **1998**, *10*, 3769.
(7) Gilman, J. W.; Jackson, C. L.; Morgan, A. B.; Hayyis, R., Jr.; Manias, E.; Giannelis, E. P.; Wuthenow, M.; Hilton, D.; Phillips, S. H. *Chem. Mater.* **2000**, *12*, 1866.
(8) Yeh, J.-M.; Liou, S.-J.; Lai, C.-Y.; Wu, P.-C.; Tsai, T.-Y. *Chem. Mater.* **2001**, *13*, 1131.

Table 1. Relations of the Composition of PMMA−MMT Clay Nanocomposite Materials with the E_{corr}, R_p, i_{corr}, and R_{corr} Measured from Electrochemical Methods[a]

compound code	feed composition (wt %)		inorganic content found in product[b] (wt %)	electrochemical corrosion measurements				
	PMMA	MMT		E_{corr} (mV)	R_p (kΩ·cm^2)	i_{corr} (nA/cm^2)	R_{corr} (MPY)	thickness[c] (μm)
bare				−604	2.7	1.9×10^4	36.7	
PMMA	100	0	0	−485	3.2×10^2	1.2×10^2	2.3×10^{-1}	110
CLMA1	99	1	1.2	−379	9.2×10^2	4.5×10^1	8.0×10^{-2}	112
CLMA3	97	3	3.5	−278	6.4×10^3	9.4	1.8×10^{-2}	121
CLMA5	95	5	6.9	−78	7.5×10^3	5.7	1.1×10^{-2}	113
CLMA10	90	10	18.1	−19	1.8×10^4	2.3	4.4×10^{-3}	117
CLMA-N10	90	10	22.1					

[a] A saturated calomel electrode was employed as the reference electrode. [b] As determined form TGA measurements. [c] As measured by a digimatic micrometer.

filtering the solution in a Buchner funnel. Purification of products was performed by washing and filtering samples repeatedly at least three times to remove any excess of ammonium ions.

Preparation of Poly(methyl methacrylate)−Clay Nanocomposites. As a typical procedure for the preparation of the PCN materials with 1 wt % clay loading, first, an appropriate amount of organophilic clay (0.1 g) was introduced into 100 mL of toluene under magnetic stirring overnight at room temperature; 9.9 g of methyl methacrylate monomer was subsequently added to the solution, which was stirred for another 24 h. Upon addition of benzoyl peroxide (0.224 g), the solution was stirred for 5 h at 80 °C under a N_2 atmosphere. The as-synthesized lamellar nanocomposite precipitates were then obtained by precipitating from an excess amount of *n*-hexane (800 mL) and by subsequent drying under dynamic vacuum at room temperature for 48 h.

Polymer Recovery (Extraction). A reverse cationic-exchange reaction was employed to separate bound PMMA from the inorganic component in the nanocomposite.[9] As a typical extraction procedure, 2 g of fine powder of as-synthesized PCN fine powders was dissolved in ≈100 mL of tetrahydrofuran (Beaker A). Separately, 10 mL of stock solution of 1 wt % $LiCl_{(s)}$ in tetrahydrofuran was prepared (Beaker B). Both beakers were under vigorous magnetic stirring for 3−4 h at room temperature. After the contents of the two beakers were combined, the mixture was stirred overnight followed by Soxhlet extraction at 80 °C for 24 h. Extract solution was then poured into an excess amount of *n*-hexane to precipitate the polymer. After filtration, the polymer was dried under vacuum at room temperature for 48 h. Molecular weights of both extracted and bulk PMMA were determined by gel permeation chromatography analyses with THF as the eluant.

Preparation of Coatings and Electrochemical Measurements. The PMMA and PCN fine powder were dissolved in NMP, instead of THF, to give typically 1 wt % solutions for improving the film formation. The solutions were cast dropwise onto the cold-rolled steel (CRS) coupons (1.0 × 1.0 cm) followed by drying in air for 24 h at 40 °C to give coatings of ≈115 μm, measured by a digimatic micrometer (Mitutoyo), in thickness. The coating ability of PCN on CRS was similar to that of bulk PMMA. The coated and uncoated coupons were then mounted on the working electrode so that only the coated side of the coupon was in direct contact with the electrolyte. The edges of the coupons were sealed with super fast epoxy cement (SPAR). All the electrochemical measurements of corrosion potential, polarization resistance, and corrosion current were performed on a VoltaLab model 21 potentiostat/galvanostat and repeated at least three times. The electrolyte was NaCl (5 wt %) aqueous solution. The open circuit potential (OCP) at the equilibrium state of the system was recorded as the corrosion potential (E_{corr} in V vs SCE). The polarization resistance (R_p in Ω/cm^2) was measured by sweeping the applied potential from 20 mV below to 20 mV above the E_{corr} at a scan rate of 500 mV/min and by recording the corresponding current change. The R_p value was obtained from the slope of the potential−current plot. The Tafel plots were obtained by the scanning potential from 250 mV below to 250 mV above the E_{corr} at a scan rate of 500 mV/min. The corrosion current (i_{corr}) was determined by superimposing a straight line along the linear portion of the cathodic or anodic curve and extrapolating it through E_{corr}. The corrosion rate (R_{corr}, in milli-inches per year, MPY) was calculated from the following equation:

$$R_{corr}(\text{MPY}) = [0.13 i_{corr}(\text{E.W.})]/[A \cdot d]$$

where E.W. is the equivalent weight (in g/equiv), A is the area (in cm^2), and d is the density (in g/cm^3).

A VoltaLab model 40 potentiostat/galvanstat was employed to perform the impedance spectroscopy studies. Impedance measurements were carried out in the frequency range 100 kHz to 100 mHz. The working electrode was first maintained in the test environment for 30 min to reach an equilibrium state before the impedance run. This served to put the electrode in a reproducible initial state and to make sure that no blistering occurred during the conditioning period. All experiments were performed at a room temperature of 25 ± 1 °C. All data were replicated at least three times to ensure reproducibility and statistical significance.

Preparation of Free-Standing Films and Barrier Property Measurements. To enhance the mechanical strength of free-standing film of as-synthesized materials for molecular (H_2O and O_2) barrier property measurements under high-pressure difference conditions, a commercial PMMA with high molecular weight (M_w = 350 000) was blended into the casting solution for film formation. Typically, 0.1 g of as-synthesized PMMA or PCN materials blended with 0.1 g of commercialized PMMA was dissolved in 10 mL of NMP under magnetic stirring at room temperature for 4 h. The solution was cast onto a substrate (e.g., a microscope glass slide). The solvent was allowed to evaporate at 90−100 °C under a hood for 24 h. The sample-coated glass substrate was then immersed into the distilled water for 24 h to give the free-standing film of PMMA and PCN materials. Oxygen permeabilities of free-standing film (or called membrane) were determined by using the Yanco GTR-10 gas permeability analyzer. The gas permeability was measured by the following equation:

$$P = l/(p_1 - p_2) \times \frac{q/t}{A}$$

where P is the gas permeability [cm^3(STP)·cm/cm^2·s·cmHg], q/t is the volumetric flow rate of the gas permeate [cm^3(STP)/s], l is the free-standing film thickness [cm], A is the effective free-standing film area [cm^2], and p_1 and p_2 are the pressures [cmHg] on the high-pressure and low-pressure sides of the free-standing film, respectively. The rate of transmission of O_2 was obtained by gas chromatography from which the air permeability was calculated. On the other hand, the experiment of water vapor permeation was carried out by using the same apparatus as pervaporation except that the feed solution was not in contact with the membrane. The setup is shown in

(9) Meier, L. P.; Sheldon, R. A.; Caseri, W. R.; Suter, U. W. *Macromolecules* **1994**, *27*, 1637.

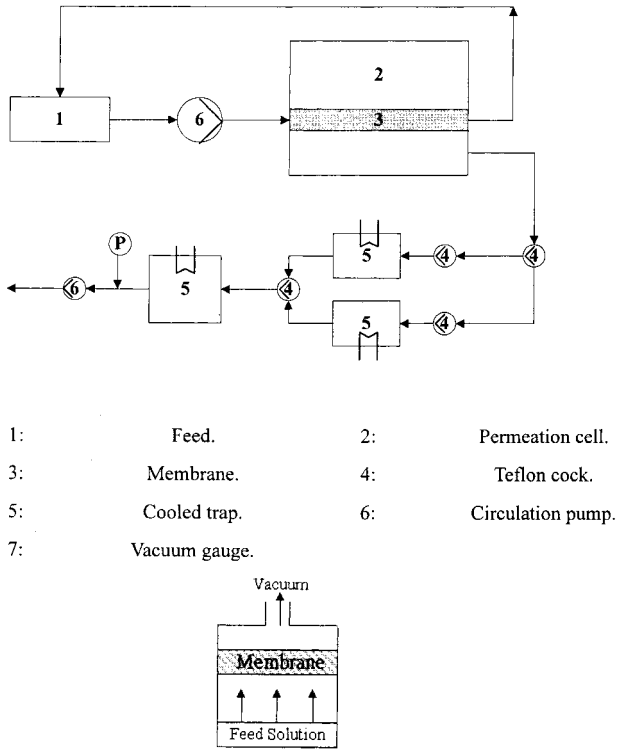

Figure 1. Vapor permeation apparatus.

Figure 1. The feed solution was vaporized first and subsequently permeated through the membrane with an effective area of ≈10.2 cm^2. The permeation rate was determined by measuring the weight of the permeate.

Results and Discussions

Montmorillonite (MMT) is a clay mineral containing stacked silicate sheets measuring ≈10 Å in thickness and ≈2180 Å in length.[10] It possesses a high aspect ratio (about 220) and a platey morphology. MMT has a high swelling capacity, which is important for efficient intercalation of the polymer, and is composed of stacked silicate sheets that offer enhanced thermal stability, mechanical strength, fire retardant, and molecular barrier properties.

To synthesize the PCN materials, organophilic clay was first prepared by a cation-exchange reaction between the sodium cations of MMT clay and alkylammonium or alkylphosphonium ions of intercalating agent. Organic MMA monomers were subsequently intercalated into the interlayer regions of organophilic clay hosts followed by a typical free-radical polymerization. The composition of the PCN materials was varied from 0 to 10 wt % of clay with respect to PMMA content as summarized in Table 1.

Characterization. The representative FTIR spectra of the organophilic clay, bulk PMMA, and PCN materials are shown in Figure 2. The characteristic vibration bands of PMMA are at 1450 cm^{-1} (C−O) and 1730 cm^{-1} (C═O), and those of MMT clay are shown at 1040 cm^{-1} (Si−O), 600 cm^{-1} (Al−O), and 420 cm^{-1} (Mg−O).[11] As the loading of MMT clay is increased, the intensities of

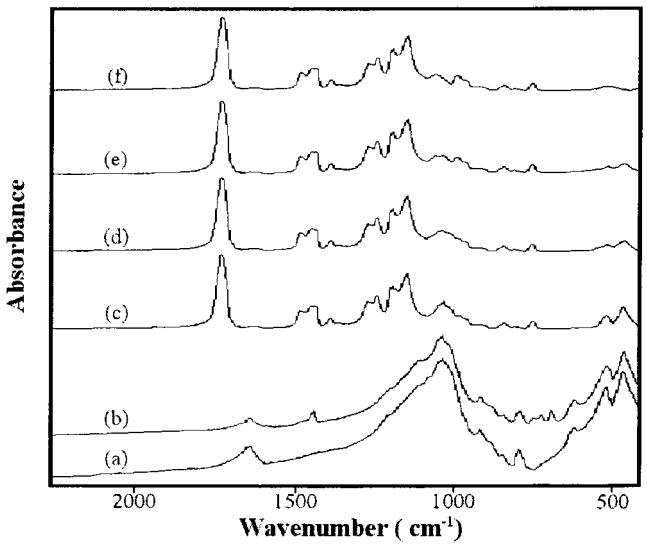

Figure 2. FTIR spectra of (a) clay, (b) organophilic clay, (c) CLMA1, (d) CLMA3, (e) CLMA5, and (f) CLMA10.

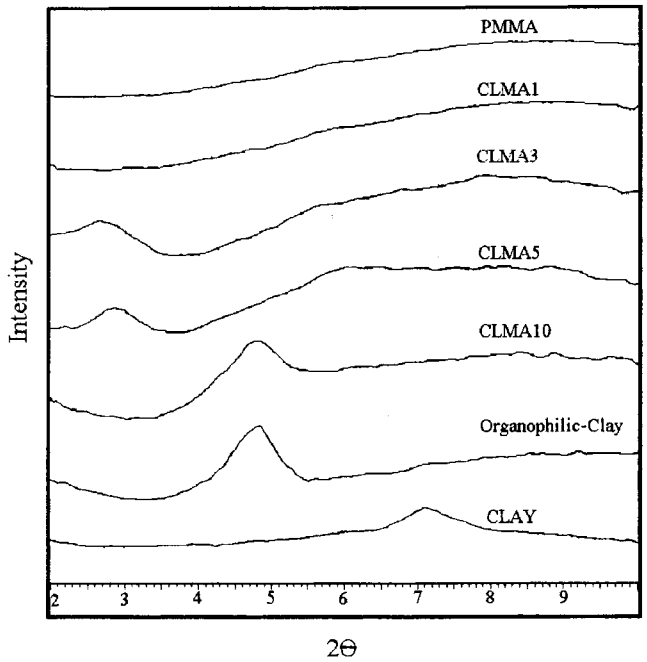

Figure 3. Wide-angle powder X-ray diffraction patterns of organophilic clay, PMMA, and a series of PMMA−clay nanocomposite materials.

MMT clay bands become stronger in the FTIR spectra of PCN materials. Figure 3 shows the wide-angle powder X-ray diffraction patterns of organophilic clay and a series of PCN materials. For CLMA1, there is a lack of any diffraction peak in $2\theta = 2-10°$ as opposed to the diffraction peak at $2\theta = 4.85°$ (d spacing = 1.82 nm) for organophilic clay, indicating the possibility of having exfoliated silicate nanolayers of organophilic clay dispersed in a PMMA matrix. When the amount of organoclay increased to 5%, there was a small peak appearing at $2\theta = 2.8°$, corresponding to a d spacing of 3.15 nm. This implied that there is a small amount of organoclay that cannot be exfoliated in the PMMA and existed in the form of an intercalated layer structure. For CLMA10, the interlayer distance of organoclay nanolayers cannot be further increased and displayed a d spacing of organophilic clay in the organic PMMA

(10) Yano, K.; Usuki, A.; Okada, A. *J. Polym. Sci., Polym. Chem. Ed.* **1997**, *35*, 2289.
(11) Kim, J. W.; Choi, H. J.; Jhon, M. S. *Macromol. Symp.* **2000**, *155*, 229.

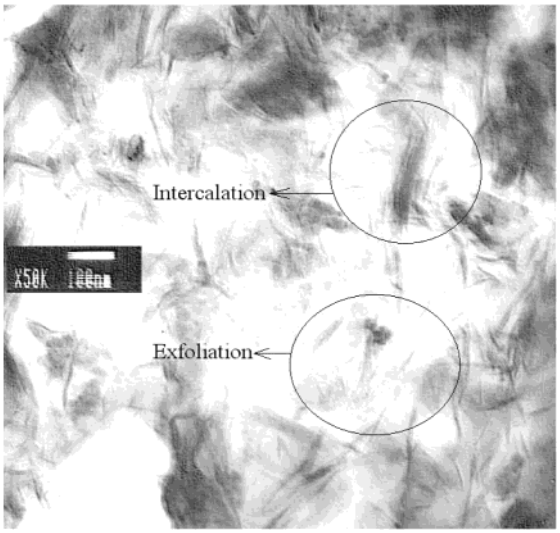

Figure 4. Transmission electron microscopy of CLMA5.

Table 2. Molecular Weights of Bulk and Extracted PMMA

sample	M_w	M_n	M_w/M_n	sample	M_w	M_n	M_w/M_n
PMMA	39 400	14 200	2.77	CLMA5	23 200	13 900	1.66
CLMA1	35 800	15 300	2.33	CLMA10	22 400	12 900	1.73
CLMA3	25 800	14 400	1.79				

matrix, indicating that a large amount of organoclay existed in an intercalated layer structure. In Figure 4, the TEM of PCN materials with 5 wt % clay loading reveals that the nanocomposite displays a mixed nanomorphology. Individual silicate layers, along with two- and three-layer stacks, are found to be exfoliated in the PMMA matrix. In addition, some larger intercalated tactoids can also be identified.

***M_w* Determination of Extracted and Bulk PMMA.** Molecular weights of the various polymer samples recovered from the nanolayers of MMT clays were obtained by gel permeation chromatography analyses eith THF as the eluant. All of the GPC elution pattern of samples displayed a single peak, corresponding to a molecular weight value, as summarized in Table 2. The molecular weights of extracted PMMA were found to be slightly lower than that of the bulk PMMA, indicating

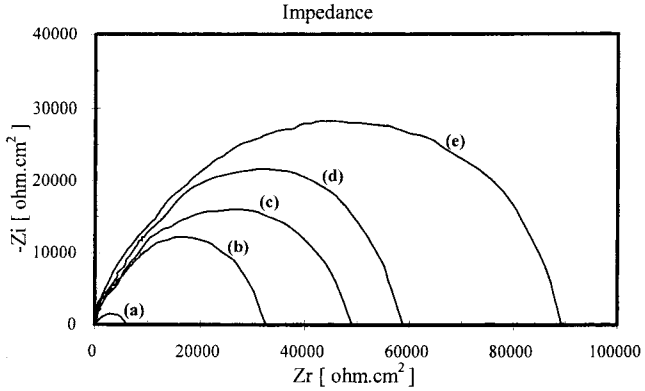

Figure 6. Nyquist plot of five CRS samples in 5 wt % NaCl aqueous solution (a) PMMA-coated, (b) CLMA1-coated, (c) CLMA3-coated, (d) CLMA5-coated, and (e) CLMA10-coated.

the structurally restricted polymerization situations in the intragallery region of the MMT clay[12] and/or the nature of clay−oligomer interactions, such as adsorption, during the polymerization reaction.

Anticorrosion Performance of Coatings. Anticorrosive performance of sample-coated CRS coupons can be examined from the values of corrosion potential (E_{corr}), polarization resistance (R_p), corrosion current (i_{corr}), and corrosion rate (R_{corr}), as listed in Table 1. The CRS coupon coated with PMMA shows a higher E_{corr} value than the uncoated CRS. However, it exhibits a lower E_{corr} value than the specimen coated with PCN materials. For example, the CLMA1-coated CRS has a high corrosion potential of ca. −379 mV at 30 min. Even after 5 h of measurement, the potential remained at ca. −385 mV. Such a E_{corr} value implies that the CLMA1-coated CRS is more noble toward the electrochemical corrosion compared to the PMMA. The CLMA1-coated CRS shows a polarization resistance (R_p) value of 9.2×10^2 kΩ/cm^2 in 5 wt % NaCl, which is about 2 orders of magnitude greater than the uncoated CRS. The Tafel plots for (a) uncoated, (b) PMMA-coated, (c) CLMA1-coated, (d) CLMA3-coated, (e) CLMA5-coated, and (f) CLMA10-coated CRS are shown in Figure 5. For example, the corrosion current (i_{corr}) of CLMA1-coated CRS is ca. 45 nA/cm^2, which corresponds to a corrosion

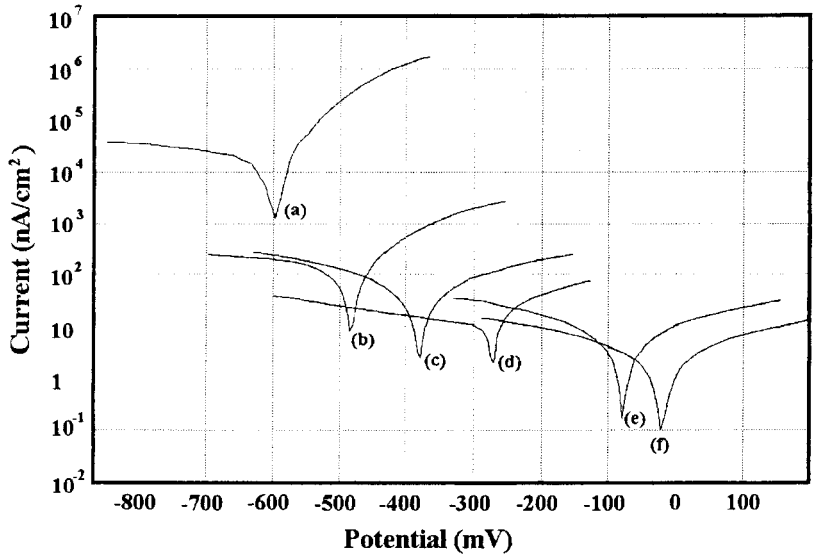

Figure 5. Tafel plots for (a) uncoated, (b) PMMA-coated, (c) CLMA1-coated, (d) CLMA3-coated, (e) CLMA5-coated, and (f) CLMA10-coated CRS measured in 5 wt % NaCl aqueous solution.

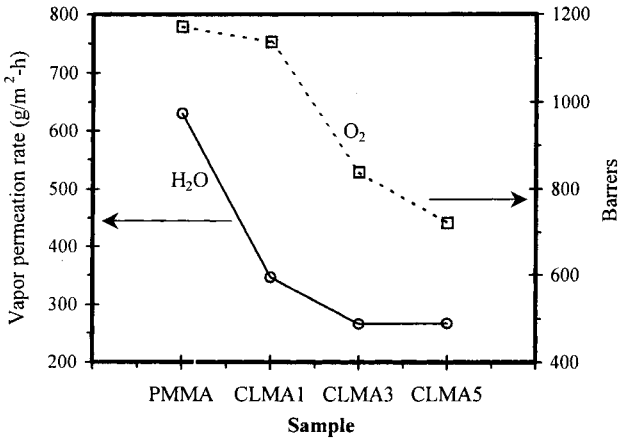

Figure 7. Permeability of H_2O and O_2 as a function of the MMT clay content in the PMMA−clay nanocomposite materials.

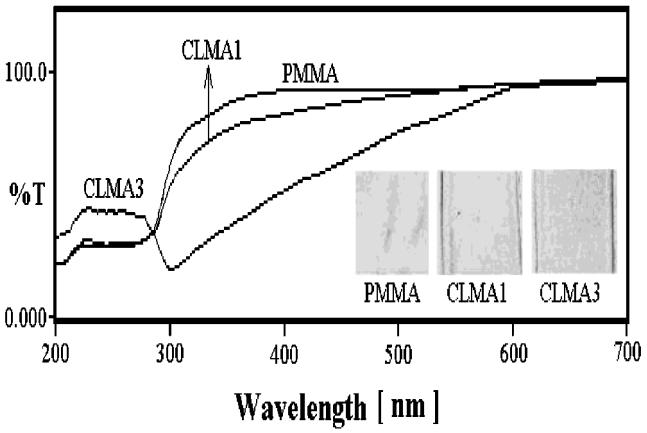

Figure 8. UV−Visible transmission spectra of PMMA and PMMA−clay nanocomposite containing 1 and 3 wt % MMT.

rate (R_{corr}) of ca. 8.0×10^{-2} MPY (Table 1). Electrochemical corrosion current values of PCN materials as coatings on CRS were found to decrease gradually with a further increase in clay loading.

Electrochemical impedance spectroscopy (EIS) was also used to examine the activity difference between the CRS surface after PMMA and PCN materials treatment. To this end five samples were prepared. The first sample (a) was PMMA-coated CRS. A series of samples denoted with (b), (c), (d), and (e) were CRS-coated by PCN materials with different clay loadings. The corrosion of these samples in 5 wt % NaCl aqueous electrolyte for 30 min was followed by EIS. Figure 6 shows the Nyquist plots of the five samples. The charge-transfer resistances of samples (a), (b), (c), (d), and (e) as determined by the intersection of the low-frequency end of the semicircle arc with the real axis are 5 000, 32 000, 49 000, 58 000, and 89 000 $\Omega \cdot cm^2$, respectively.[1] The results clearly demonstrate that the sample with the highest clay loading has the greatest anticorrosive performance. This novel property of enhanced anticorrosion effect for PMMA−clay nanocomposite materials compared to that of bulk PMMA might have arisen from dispersing silicate nanolayers of clay in a PMMA matrix to increase the tortousity of the diffusion pathway of oxygen and water. This is further evidenced by the studies of the O_2 and H_2O molecular barrier effect as discussed in the following section.

Molecular Barrier and Optical Clarity of Free-Standing Films. The free-standing films (or called membranes) of PCN materials and bulk PMMA used for the molecular barrier measurements were prepared to have film thicknesses of ≈50 μm. Compared to that of PMMA, free-standing film of PCN materials at low clay loading (e.g., 3 wt %) shows about 57 and 28% reduction of H_2O and O_2 permeability, respectively, as shown in Figure 7. Furthermore, it should be noted that a further increase of clay loading results in a slightly further enhanced molecular barrier property of bulk PCN materials. On the other hand, because of the nanoscale dispersion of the clays in the PMMA matrix, optical clarity remains high at low clay contents (e.g., CLMA1), which yield primarily exfoliated composites.[13,14] Figure 8 shows the UV/vis transmission spectra of pure PMMA and PMMA−clay nanocomposites with 1 and 3 wt % MMT. These films have thickness of ≈180 μm. The spectra of CLMA1 show that the visible region (400−700 nm) is nearly not affected by the presence of

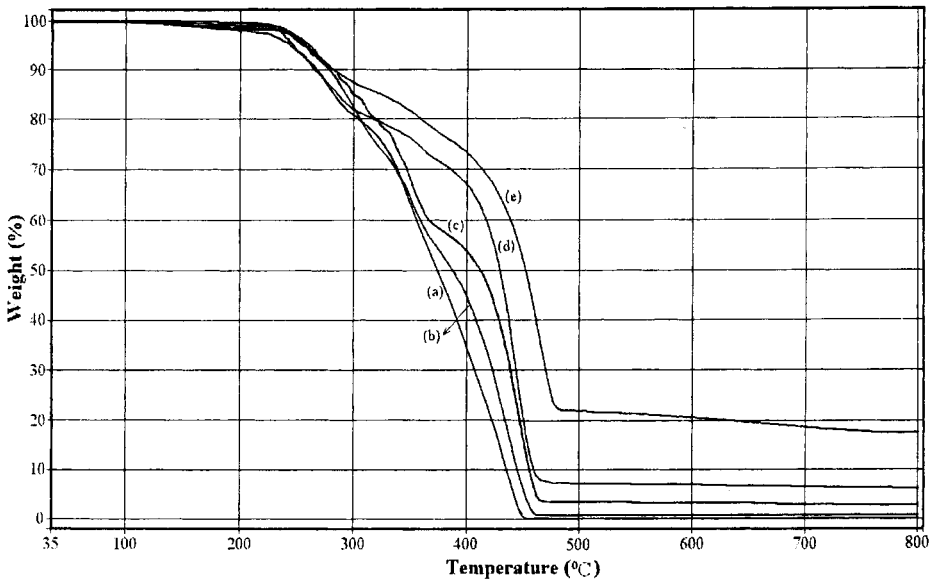

Figure 9. TGA curves of (a) PMMA, (b) CLMA1, (c) CLMA3, (d) CLMA5, and (e) CLMA10.

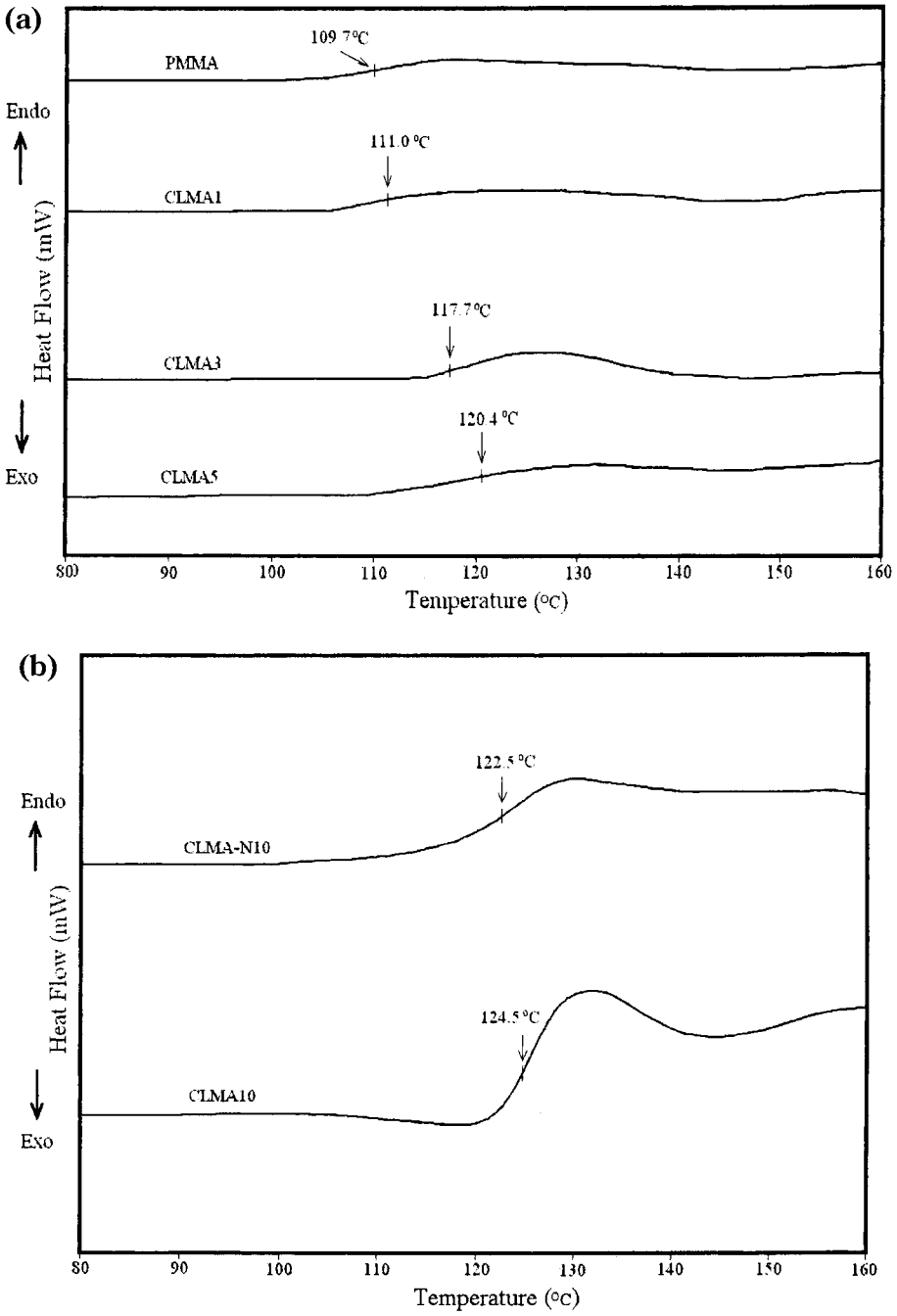

Figure 10. (a) DSC curves of PMMA and a series of PMMA−clay nanocomposite materials; (b) DSC curves of PMMA−clay nanocomposite materials with two different intercalating agents.

the clay and retains the high transparency of the PMMA. However, the spectra of CLMA3 exhibiting low transparency of the PMMA reflect the primarily intercalated composites. For the ultraviolet wavelength, there is strong scattering and/or absorption, resulting in very low transmission of the UV light.

Thermal Properties of Fine Powders. Figure 9 shows typical TGA thermograms of weight loss as a function of temperature for PMMA and the PCN materials, as measured under an air atmosphere. In general, there appeared to be several stages of weight loss starting at ≈200 °C and ending at 800 °C, which might correspond to the degradation of the intercalating agent followed by the structural decomposition of the polymers. Evidently, the thermal decomposition of those PCN materials shifted toward the higher temperature range than that of PMMA, which confirms the enhancement of thermal stability of intercalated PMMA.[15] DSC traces of the Pure PMMA and PCN materials are shown in Figure 10 a,b. The pure PMMA exhibits an endotherm at 109.7 °C, corresponding to the T_g of PMMA.[16] All the PCN materials show an increased T_g compared to pure PMMA, as shown in Figure 10a. This is

(12) Wrobleski, D. A.; Benicewicz, B. C.; Thompson, K. G.; Byran, C. J. *Polym. Prepr. (Am. Chem. Soc., Div. Polym. Chem.)* **1994**, *35* (1), 265.
(13) Wu, C.-G.; DeGroot, D. C.; Marcy, H. O.; Schindler, J. L.; Kannewurf, C. R.; Liu, Y.-J.; Hirpo, W.; Kanatzidis, M. G. *Chem. Mater.* **1996**, *8*, 1992.
(14) Strawhecker, K. E.; Manias, E. *Chem. Mater.* **2000**, *12*, 2943.
(15) Lee, D. C.; Jang, L. W. *J. Appl. Polym. Sci.* **1996**, *61*, 1117.
(16) Brandrup, J.; Immurgut, E. H. *Polymer Handbook*, 3rd ed.; Wiley-Interscience: New York, 1989; pp VI-219.

tentatively attributed to the confinement of the intercalated polymer chains within the clay galleries that prevent the segmental motions of the polymer chains. We also found, in these studies, that the PCN materials with quaternary alkyphosphonium salt as the intercalating agent displayed a little bit higher T_g than that with conventional alkylammonium intercalating agent, as shown in Figure 10b.

Concluding Remarks

A series of polymer−clay nanocomposite (PCN) materials were prepared by effectively dispersing the inorganic nanolayers of MMT clay in an organic PMMA matrix via in situ thermal polymerization. Organic methyl methacrylate monomers were first intercalated into the interlayer regions of organophilic clay hosts followed by a typical free-radical polymerization. The as-synthesized PCN materials were characterized by infrared spectroscopy, wide-angle powder X-ray diffraction, and transmission electron microscopy. PCN coatings with low clay loading (e.g., 1 wt %) on cold-rolled steel (CRS) were found to be superior in anticorrosion over those of bulk PMMA on the basis of a series of electrochemical measurements of corrosion potential, polarization resistance, corrosion current, and impedance spectroscopy in 5 wt % aqueous NaCl electrolyte. Enhanced anticorrosion of PMMA−clay nanocomposite materials compared to bulk PMMA might have resulted from dispersing silicate nanolayers of clay in the PMMA matrix to increase the tortousity of the diffusion pathway of oxygen and water. The molecular weights of PMMA extracted from PCN materials and bulk PMMA were determined by gel permeation chromatography (GPC) with tetrahydrofuran as the eluant. The molecular weights of extracted PMMA were found to be slightly lower than that of the bulk PMMA, indicating the structurally restricted polymerization situations in the intragallery region of the MMT clay and/or the nature of clay−oligomer interactions, such as adsorption, during the polymerization reaction. Effects of the material composition on the molecular barrier, optical clarity, and thermal stability of PMMA along with PCN materials, in the form of both free-standing film and fine powder, were also studied by molecular permeability analysis, ultraviolet−visible transmission spectra, differential scanning calorimetry (DSC), and thermogravimetric analysis (TGA). The free-standing film (or called membrane) of PCN materials at low clay loading (e.g., 3 wt %) compared to PMMA shows about 57 and 28% reduction of H_2O and O_2 permeability, respectively. Optical clarity of PCN material remains high at low clay contents (e.g., CLAM1), which yield primarily exfoliated composites. Thermal decomposition of those PCN materials shifted toward the higher temperature range than that of PMMA on the basis of the TGA studies, which confirms the enhancement of the thermal stability of intercalated PMMA. All the PCN materials show an increased T_g compared to pure PMMA based on the DSC studies. This is tentatively attributed to the confinement of the intercalated polymer chains within the clay galleries that prevents the segmental motions of the polymer chains.

Acknowledgment. The financial support of this research by the NSC 89-2113-M-033-014 is gratefully acknowledged.

CM010337F